



HAL
open science

AgTi(C, N)-based coatings for biomedical applications: influence of silver content on the structural properties

N K Manninen, R Escobar Galindo, N Benito, N M Figueiredo, A Cavaleiro,
C Palacio, S Carvalho

► **To cite this version:**

N K Manninen, R Escobar Galindo, N Benito, N M Figueiredo, A Cavaleiro, et al.. AgTi(C, N)-based coatings for biomedical applications: influence of silver content on the structural properties. Journal of Physics D: Applied Physics, 2011, 44 (37), pp.375501. 10.1088/0022-3727/44/37/375501 . hal-00654139

HAL Id: hal-00654139

<https://hal.science/hal-00654139>

Submitted on 21 Dec 2011

HAL is a multi-disciplinary open access archive for the deposit and dissemination of scientific research documents, whether they are published or not. The documents may come from teaching and research institutions in France or abroad, or from public or private research centers.

L'archive ouverte pluridisciplinaire **HAL**, est destinée au dépôt et à la diffusion de documents scientifiques de niveau recherche, publiés ou non, émanant des établissements d'enseignement et de recherche français ou étrangers, des laboratoires publics ou privés.

Ag-Ti(C, N)-based coatings for biomedical applications: influence of silver content on the structural properties

N. K. Manninen¹, R. Escobar Galindo², N. Benito³, N.M. Figueiredo⁴, A. Cavaleiro⁴, C. Palacio³, S.Carvalho¹

¹Universidade do Minho, Dept. Física, Campus de Azurém, 4800-058 Guimarães, Portugal

² Instituto de Ciencia de Materiales de Madrid (ICMM -CSIC), Cantoblanco, 28049, Madrid, Spain

³ Departamento de Física Aplicada (CXII), Universidad Autónoma de Madrid, Cantoblanco, 28049, Madrid, Spain

⁴SEG-CEMUC Mechanical Engineering Department, University of Coimbra, 3030-788 Coimbra

Abstract

Ag – TiCN coatings were deposited by DC reactive magnetron sputtering and their structural and morphological properties were evaluated. Compositional analysis showed the existence of Ag-TiCN coatings with different Ag/Ti atomic ratios (ranging from 0 to 1.49). The structural and morphological properties are well correlated with the evolution of Ag/Ti atomic ratio. For the samples with low Ag/Ti atomic ratio (below 0.20) the coatings crystallize in a B1-NaCl crystal structure typical of TiC_{0.3}N_{0.7}. The increase of Ag/Ti atomic ratio promoted the formation of Ag crystalline phases as well as amorphous CN_x phases detected in both XPS and Raman Spectroscopy analysis. Simultaneously, to the formation of Ag crystalline phases and amorphous carbon based phases, a decrease in TiC_{0.3}N_{0.7} grain size was observed as well as the coatings densification.

Keywords: Sputtering, XPS, Raman, TEM

1. Introduction

The increasing demand for sustainable products requires the development of new knowledge-based materials with advanced properties. These products are then expected to: last longer, have a better performance, be safe, and be more efficient. These requirements, which may be seen as a rule of thumb for most known materials, gain particular importance when dealing with applications involving the human body: the so-called biomaterials [1]. Fatigue fracture and wear have been identified as major problems associated with implant loosening, stress-shielding and ultimate implant failure. Also, medical devices have sometimes to be physically removed due to infection. In fact, these wear-related problems are being studied by the development of new functional biomaterials which can intend to have some improved physical, mechanical, tribological or biological properties [2-4]. The tendency in implant science is to replace the total hip prosthesis, which was usually made of a variety of materials such as metals, ceramics, polymers and composites, by those materials coated with protective thin-films.

Different types of PVD hard ceramic coatings were frequently considered as possible solutions to overcome the drawbacks mentioned above. In recent years, nanocomposite protective films have gained popularity due to their superior mechanical and tribological properties compared to traditional single-phase films. Superhard nanocomposites based on the combination of various transition metal nitrides, carbides and carbonitrides have been reported in last years [5-8]. Clearly control the nanoscale coating structure in order to achieved the best properties (enhanced hardness and tribological behavior) is the main motivation of these reports. Titanium carbonitride (TiCN) presents excellent wear resistance, high hardness and good corrosion resistance beyond its non-cytotoxic character. These properties justify that TiCN could be a potential coating for hip implants. TiCN has been studied in last decades specially the structural properties and their relation with the mechanical and tribological behavior, which determines the in-service performance in mechanical applications [3,4,9,10]. As example, *Martínez-Martínez et al.* reported that in TiCN coatings deposited by magnetron sputtering, a C enrichment led to the formation of an amorphous carbon phase that can help to decrease the friction coefficient and the wear rate, although promoting a hardness reduction, conditions giving the best performance in some applications, such as in hip implants [11].

Previous results obtained demonstrated that although these type of biomaterials presented good mechanical properties and low cytotoxicity [3,12] they were prone to be colonized by *Staphylococcus epidermidis*. Hence this strengthens the urgent need of improving coatings incorporating antimicrobial properties. The current investigations supports that use of silver ion or metallic silver as well as silver nanoparticles can be exploited in medicine for burn treatment, dental materials, coatings stainless steel materials, textile fabrics, water treatment, sunscreen lotions and posses low toxicity to human cells [13,14].

Indeed, several studies have been performed describing the use of silver for biomedical applications [15-17]. However, they only consider silver antimicrobial action disregarding how silver is incorporated and/or its morphology. In fact the antiomicrobial property of silver is related to the amount of silver and the rate of silver released is correlated with structural properties.

The aim of the present study is the production and structural characterization of Ag-TiCN for hip implant applications and the focus is to study the influence of silver addition to the structure of TiCN coatings produced by DC reactive magnetron sputtering. According to the results obtained by several authors, the functional properties are strongly correlated with the coatings structure. On the one hand the mechanical/tribological behaviors are clearly governed by the balance between crystalline and amorphous phases. On the other hand, silver antimicrobial properties are mainly controlled by the amount of silver present in the system and by the surface to volume ratio, which depends on the morphology of silver clusters. Thus, in order to understand the functional properties of Ag-TiCN the knowledge of structure and morphology is primordial. In fact a deep investigation of the structure needs to be done first in order to understand the usually very complex results one obtains from tribological and biological tests. This work intends to contribute to this comprehension field.

2. Materials and Methods

Ag-TiCN samples were deposited by reactive DC magnetron sputtering from a high-purity Ti target (200 x 100 mm²) onto polished and ultrasonically cleaned 316 L

stainless steel (20 x 20 mm²) and single crystalline silicon (100). High purity silver is incorporated on a second Ti target in the form of nuggets. Two series of samples were deposited using this Ti target with 6 and 14 Ag nuggets, resulting in relative Ag sputtering areas (only the preferential eroded zone of the target is considered) of 15% and 43%, respectively.

To further vary the Ag content in the films in both series the current density applied to each target was also changed. The substrates were previously sputter-etched for 20 minutes in an Ar⁺ atmosphere. The depositions were carried out in Ar+C₂H₂+N₂ mixtures using an Alcatel SCM650 apparatus, with the substrates rotating at 70 mm over the target at a constant speed of 8 rpm. The base pressure in the deposition chamber was about 10⁻³ Pa and rose up to values between 3.1 x10⁻¹ and 4.7x10⁻¹ Pa during the depositions. The films were grown at a constant temperature (573 K) and bias voltage (-70 V). Argon flow was kept constant at 60 sccm while the reactive gases fluxes (C₂H₂ and N₂) were changed as it is indicated in Table 1. The variation on the reactive gases fluxes was performed in order to maintain approximately constant the C and the N contents, although the density current applied to the targets was changed. The stoichiometry of the deposited films was investigated by a Cameca SX 50 Electron Probe Microanalysis (EPMA) apparatus. Ball crater tests were used to measure the film thickness. The structure and phase distribution of the coatings were determined by X-ray diffraction (XRD) using a conventional Philips PW 1710 diffractometer, operating with Cu K α radiation in grazing incidence mode (angle of incidence of 1.5°).

The microstructure analysis was carried out on Tecnai G2 transmission electron microscope operated at 200 kV. The morphology of the coatings was evaluated by Scanning Electron Microscopy (EDAX-Nova nanoSEM 200).

In order to analyze the chemical bonding Raman Spectroscopy and X-ray Photoelectron Spectroscopy (XPS) were performed. Raman spectra were acquired with a Renishaw InVia Microscope. The excitation light was the 514.5 nm line of an Ar laser.

XPS spectra were acquired using a hemispherical analyzer (SPECS EA-10 Plus). The pass energy was 15 eV giving a constant resolution of 0.9 eV. The Ag 3d_{5/2} line at 367.9 eV was used in order to calibrate the binding energies. A twin anode (Mg and Al) X-ray source was operated at a constant power of 300 W using Al K α radiation. The samples were sputter-cleaned in situ using a broad 3 keV Ar⁺ beam for 10 minutes. Due

to the large dispersion of reference peak values found in the literature, XPS analysis of TiN, TiC and TiO₂ reference samples was performed to obtain experimentally the binding energies of interest. In Figure 1 the Ti2p spectra of the reference samples is presented clearly showing the doublets for TiC (454.6, 460.4 eV), TiN (455.4, 461.2 eV) and TiO₂ (458.5, 464.2 eV). In the TiN and TiC samples we also have found a doublet at (456.6, 462.3 eV) that some authors have associated to Ti₂O₃ [18]. We have labeled it here as TiO_x as it might include other titanium oxidation states. It is worth noting that the separation of the Ti2p_{3/2} and Ti2p_{1/2} components for the oxide doublets is 5.7 eV, while for the nitride and carbide is 5.8 eV. This is in very good agreement with the theoretical values expected. In Table 2 the binding energies of the C1s, N1s, Ti2p and O1s bands found for the reference samples are summarized and they will be used in the discussion of the XPS results.

3. Results and Discussion

3.1. Deposition Rate and Chemical Composition

The synthesis conditions together with the chemical composition and the thickness of the coatings are summarized in Table 1. The film thicknesses ranged from 1.4 to 3.2 μm. The deposition rate tends to increase with the increment of $J_{Ti+Ag} + J_{Ti}$, as it is clearly seen on Figure 2. However, for the first series a poisoning effect is observed in the sample with the highest current density. This is probably due to the simultaneous increase in the flow of reactive gases with the current density. In the inset on Figure 2, it is possible to observe the voltage increase in both targets during the deposition of the sample processed with $J_{Ti+Ag} + J_{Ti}$ of 16 mA/cm². The target voltage increase is due to the change of the target surface condition. In fact, due to the presence of reactive gases (N₂ + C₂H₂), both TiN and TiC layers should be formed at the Ti surface targets (**phenomenon called poisoning effect**). Since the sputtering yield of both compounds is lower than that of Ti, a decrease in the deposition rate is consequently observed [19,20]. Concerning the others depositions no significant changes on the targets voltage values were observed during the deposition time.

Also, it is possible to observe that the increment on the target voltage is higher for the TiAg target than for the Ti target. This effect cannot be explained from the formation of

a silver nitride phase on the target surface, since silver is a poor nitride former. *Depla et al.* justify the increment on the target voltage during sputtering of silver target in an Ar/N₂ plasma, by the presence on non-reacted N atoms in the target top surface layers [21].

The chemical composition of the samples deposited onto silicon, measured by EPMA is also given in Table 1. The compositional analysis shows that by increasing the J_{TiAg}/J_{Ti} ratio for the first series the Ti content in the coatings decreased from 37 to 32 at. % along with an increase of the Ag content from 0 to 6 at. %. The C and N content do not change significantly with the synthesis conditions. In the 2nd series, the increase of Ag area, promotes an increase in the silver contents in the coatings. The silver content changes from 11 to 27 at. % while Ti content decreased from 27 to 18 at. %. It can be seen that the current density applied to each magnetron (J_{TiAg} and J_{Ti}) is the driven parameter for the film chemical composition. To that respect, Figure 3 shows the variation of the Ag/Ti ratio versus J_{TiAg}/J_{Ti} ratio. It is observed that in the second series, the raise of Ag/Ti ratio by increasing the current applied on Ti+Ag target is faster than in the first series. In the first series, this increase is lower due the smaller erosion area of Ag on Ti target. This means that it is not only the silver content that should control the films properties but also the Ag/Ti atomic ratio.

3.2. Phase Formation

XRD analysis was carried out in order to understand the evolution of the structure with the variation of Ag/Ti atomic ratio. The XRD patterns are shown in Figure 4 and the main identified crystalline phases are depicted, namely TiC_{0.3}N_{0.7} (ICDD card nr. 00-042-1488) and Ag (ICDD card nr. 00-004-0783). The differences in the chemical composition correlate well with the differences observed in the developed structure. In particular for the sample without silver the films crystallize in a B1-NaCl crystal structure typical for TiC_{0.3}N_{0.7} although a peak shift towards lower angles is denoted. This fact is in agreement with the measured chemical composition because these samples contain a slightly higher C/N atomic ratio than TiC_{0.3}N_{0.7}. Similar behavior was

observed for the samples with low Ag/Ti atomic ratio (0.06 and 0.20), although a new diffraction peak attributed to Ag (111) begins to appear.

The samples with Ag/Ti atomic ratio ≥ 0.40 exhibit also a polycrystalline structure, clearly with formation of nanosized Ag clusters. For the Ag/Ti = 0.40 sample the structure is characterized by broader peaks in the range 35 to 45°. It is difficult to unequivocally identify which phases are formed. However, in agreement for the samples with low Ag/Ti atomic ratio there are fcc phases that have the main peaks close to these values (TiCN, and Ag). It is possible to infer that the XRD patterns reveal, at least, the development of a mixture of fcc- $\text{TiC}_{0.3}\text{N}_{0.7}$ (clearly visible for lowest Ag/Ti atomic ratio) and fcc-Ag crystalline phases (clearly visible for the highest Ag/Ti atomic ratio). In fact, by increasing the Ag/Ti atomic ratio, the fcc-Ag phase becomes predominant for the Ag/Ti atomic ratio of 0.77. The increment of the Ag/Ti ratio leads to a loss of either the XRD peaks intensity and crystal size of the TiCN phase. These changes can be understood due to the interruption of the growth of TiCN phase by the nucleation of Ag nanocrystals and/or by the presence of an amorphous layer [22]. In fact, the low Ti/(C+N) ratio suggests the presence of an additional XRD amorphous phase, most likely of C or CN_x type. Indeed, these phases were also observed within the TiCN, and ZrCN systems [1,3,23]. The presence of this amorphous layer was confirmed by Raman Spectroscopy and XPS analysis.

The XRD patterns of the Ag-containing films show, even for the lowest Ag contents, evidence of crystalline Ag presence. A small bump close to 38.12° (standard position of the (111) peak of fcc Ag phase) can be detected on the 0.06 Ag/Ti film, which becomes more and more evident with the Ag content increase until give rise to well defined and progressively narrower peaks. The grain size of TiCN and Ag phases was determined by Scherrer formula taking, in both cases, the (111) peak. The calculated values varied from 15 down to 9 nm and from 5 up to 8 nm, for TiCN and Ag, respectively, with the increase of Ag/Ti. This variation should be due to the simultaneous growth of Ag, TiCN and amorphous phases. During the deposition of TiCN phase the addition of Ag and/or the presence of the C-amorphous layer cause an interrupted nucleation of the crystals, leading to smaller crystal sizes [22,24]. However, due to the great mobility of Ag atoms, the increase of the Ag content progressively leads to higher Ag crystals, explaining the inverse trends of grain size for TiCN and Ag phases. In conclusion, the coatings should

be imagined as a nanocomposite structure consisting of nanocrystals of both Ag and TiCN phases embedded in a C-rich amorphous matrix (incorporating N).

The nanocrystallinity of the Ag and TiCN grains can be confirmed by TEM cross-section observation. Fig. 5 shows the TEM micrograph of the coating with Ag/Ti = 0.40. A closer look at the Fig. 5 reveals **nanocrystallites** with sizes ranging from 5 to 17 nm. In the inset of this figure, a selected diffraction (SAD) pattern is presented. SAD pattern shows also diffuse rings where discrete spots are superimposed, revealing, as it would be expected, a nanocrystalline structure. **Two different phases, both with a fcc structure were indexed. The first phase presents a lattice parameter ($a = 0.429\text{nm}$) very close to the $\text{TiC}_{0.3}\text{N}_{0.7}$ phase (which lattice parameter stress free is 0.426 nm) while the second pattern can be indexed to Ag phase since the lattice parameter obtained by the SAD ($a = 0.408\text{ nm}$) it is close to this phase ($a = 0.409\text{ nm}$ stress free). Meanwhile, the analysis of the Debye-Scherrer rings indicates growth on (111), (200), (220), (311) and (400) planes that can be assigned with the TiCN phase and also growth on (111), (200) and (220) planes for Ag phase.**

3.3. SEM Analysis

The morphology of the coatings is disclosed by cross-sectional SEM micrographs of fractured samples and it is shown in fig. 6, **for representative samples - Ag/Ti ratios of 0 (Fig.6a); 0.20 (Fig 6b); 0.40 (Fig 6c) and 1.49 (Fig 6d).** The cross-section of the sample without silver (Fig. 6a) shows a columnar-type structure with high porosity. The low temperature during the film growth (573 K), associated with low bombardment conditions, promotes the development of this kind of structure, due to the low adatom mobility. With the increase of a second crystalline phase (Ag) and the simultaneous growth of C(N) based amorphous phases, the films became slightly less porous. For the sample with Ag/Ti of 0.40 (Fig. 6c) it is possible to see the presence of Ag nanoclusters in the boundaries of the columns near the coatings surface, which was in some way predictable, once second phases usually tend to form in grain boundaries [22]. In the sample with Ag/Ti of 1.49 (Fig. 6d) is possible to see silver clusters and some aggregates in surface (**inset on Fig.6d**).

3.4. XPS and Raman Spectroscopy

Raman Spectroscopy and XPS studies were performed on the Ag - TiCN samples, deposited on silicon substrates, with different Ag/Ti atomic ratios. XPS analysis was carried out with the aim of obtaining further information on the chemical bonding. Figure 7 shows the a) Ti2p, b) C1s, c) N1s and d) Ag3d core level XPS spectra of the deposited Ag-TiCN films with Ag/Ti atomic ratio of 0, 0.20, 0.40 and 1.49.

In Figure 7a, there are three doublets clearly identified in the Ti2p spectra of all samples. The first two doublets with Ti2p_{3/2} components centered at 458.5 and 456.6 eV respectively can be straightforwardly ascribed to TiO₂ and TiO_x bonds for all samples as derived from the analysis of the reference samples (see Figure 1 and Table 2). The oxygen impurities exeunt due to residual oxygen in the vacuum chamber, in the targets and also due to contamination after deposition. For sample without silver the third contribution is found to be at 455.1 eV (for the Ti2p_{3/2} component), that is in between the TiC (454.6 eV) and TiN (455.4 eV) bonds. This suggests the formation of a TiCN phase in good agreement with the XRD results previously shown. Similar behavior is found for sample with Ag/Ti = 0.20. However, as the silver ratio increases there is a slight but progressive shift of this third doublet towards higher binding energies. In sample with Ag/Ti = 0.40 the third doublet is centered at 455.2 eV while for Ag/Ti = 1.49 it is at 455.4 eV, namely the binding energy of TiN. This shift is therefore ascribed to a continuous decrease of the titanium bonded to carbon. The Gibbs free energy for the formation of TiN phases is – 290 kJ/mol and for TiC is – 180 kJ/mol [25]. Therefore, with the decreasing of Ti content, there is a clear trend to the formation of the thermodynamically more stable nitride phases. In fact when analyzing the C1s spectra in Figure 7b, the intensity of component ascribed to the C-Ti bonds at 282 eV decreases with the increase of the Ag/Ti ratio. In particular for sample with Ag/Ti = 1.49 this contribution simply disappears. On the other hand, for samples with high Ag/Ti ratio there is an increase of the intensity of the component ascribed to C-N bonds (286.9 eV), which is parallel to the behavior of the component assigned to N-C bonds in the N1s spectra (see below), reinforcing the idea of the formation of an amorphous C-phase incorporating N. In the N1s spectra of Figure 7c, two contributions were found at 397.0 eV and 399.2 eV ascribed to N-Ti and N-C bonds, respectively (see Table 1). The intensity of the N-C component becomes significant when the Ag/Ti increases (in agreement with the results for C1s spectra). Therefore, we can state that the presence of

CN bonds is observed in the samples with Ag/Ti atomic ratios of 0.40 and 1.49 and the appearance of these bonds are attributed to the decrease of Ti content in the coatings. The excess of C and N (low Ti/C+N) ratio, as it is possible to confirm by the composition results) promotes the formation of CN amorphous phases detected in both XPS and Raman Spectroscopy analysis (see below). Finally, from the analysis of Ag 3d photoelectron spectra (Figure 7d) it was possible to confirm that the only contribution is the Ag–Ag metal bonds, which was somehow predictable due to the low solubility of C and N in silver.

Figure 8 shows the Raman spectra of deposited Ag-TiCN samples with Ag/Ti atomic ratios 0, 0.20, 0.40 and 1.49 . The aim of Raman Spectroscopy analysis was to confirm the interpretation of structural and chemical bonding aspects done by XPS and XRD. As already discussed from the XRD analysis it is possible to observe the presence of broad peak between 35 and 45 ° for the sample with Ag/Ti atomic ratio of 0.20 and 0.40, which may be associated to the contribution of different nanocrystalline phases: TiCN and Ag, which presents three diffraction peaks between 36 and 38,6° (ICDD card nr. 21-1272). By the literature for TiN four peaks at approximately 225 (TA), 315 (LA), 450 (2A) and 550 cm⁻¹ (TO), and for TiC four peaks located at 280, 385, 585 and 675 cm⁻¹ are identified in the Raman spectra [1,3,26,27]. According to our results (Fig. 8) seems that the TiCN bonds should be located between TiN and TiC peaks.

In the region between 1250 and 1595 cm⁻¹ several authors assigned carbon phases like C–N at 1250cm-1 and C=N at 1500 cm-1 as well as D and G bands of carbon materials at 1370 and 1580 cm-1 [23,28,29]. Due to the similarity of the vibrational frequencies of C-C and C-N the interpretation of the results is difficult, due to the appearance of broad bands. Nevertheless, the Raman band around 720 cm⁻¹, that starts to appear in the sample with Ag/Ti atomic ratio of 0.40, is also associated to the presence of C–N bonds [3], which allows confirming the presence of N in the amorphous CN phases as predicted from XPS results.

4. Conclusions

Ag-TiCN thin films were deposited by reactive magnetron sputtering with different density of currents applied to the Ti and Ti+Ag targets, which controls the chemical

composition of the samples studied. The structure evolution is correlated with the Ag/Ti atomic ratio. Samples with low Ag/Ti atomic ratio (<0.20), crystallized in a B1-NaCl crystal structure typical of $\text{TiC}_{0.3}\text{N}_{0.7}$. With the increase of Ag/Ti atomic ratio a second crystalline phase begins to appear promoting a reduction in the grain size and a densification of the coatings. In samples with intermediate Ag/Ti ratio (0.20 and 0.40) the increase of silver content promotes a competitive growth between Ag and $\text{TiC}_{0.3}\text{N}_{0.7}$ phases. Simultaneously, amorphous carbon based phases begin to appear. Silver phases and CN tends to segregate in the grain boundaries of $\text{TiC}_{0.3}\text{N}_{0.7}$ causing a decrease in the grain size and a densification of the coatings. In samples with high Ag/Ti atomic ratio (>0.77), Ag appears as the dominant crystalline phase. According to the results obtained in XPS analysis, the TiCN bonds are replaced by TiN bonds as consequence of the decrease of Ti content with the increase of Ag/Ti atomic ratio. The presence of CN amorphous phases was confirmed by XPS and Raman Spectroscopy analysis.

Acknowledgements

The authors are grateful to Dr. Isabel Muñoz Ochando (Instituto de Ciencia y Tecnología de Polímeros ICTP-CSIC) for her assistance in carrying out the Raman spectroscopic analysis. The work was financially supported by Portuguese national funds through the CRUP Institution (project “Acção N° E – 1007/08) and FCT-Fundação para a Ciência e a Tecnologia, (project PTDC/CTM/102853/2008) and by the Spanish Ministry of Science and Innovation (projects FUNCOAT CSD2008-00023 and MAT2008-06618-C02). REG wish also to thank the MCINN for the financial support within the Ramón y Cajal programme. This research was partially sponsored by FEDER funds through the program COMPETE- Programa Operacional Factores de Competitividade.

References

- 1 – Oliveira C., Escobar Galindo R., Palacio C., Vasquez L., Espinosa A., Almeida B.G., Henriques M., Calderon S., Carvalho S., 2010, Thin Solid Films, 518, 5694–5699
- 2 - Mandl S. and Rauschenbach B., 2002, Surf. Coat. Technol. 156, 276-281

- 3 – Oliveira C., Gonçalves L., Almeida B.G., Tavares C.J., Carvalho S., Vaz F., Escobar Galindo R., Henriques M., Susano M., Oliveira R., 2008, *Surface and Coatings Technology*, 203, 490–494
- 4 – Geetha M., Singh A.K., Asokanami R., Gogia A.K., 2009, *Progress in Materials Science*, 54, 397 – 425
- 5 – Serro A.P., Completo C., Colaço R., Santos F., Lobato da Silva C., Cabral J.M.S., Araújo H., Pires E., Saramago B., 2009, *Surface and Coatings Technology*, 203, 3701-3707
- 6 – Tsai P.C., Chen W.J., Chen H.J., Chang C.L., 2009, *Thin Solid Films*, 517, 5044-5049
- 7 – Musil J., Vlcek J., 2001, *Surface and Coatings Technology*, 142-144, 557 - 566
- 8 – Mitterer C., Mayrhofer P.H., Musil J., 2003, *Vacuum*, 71, 279–284
- 9 - Veprek S., Zhang R.F., Veprek-Heijman M.G.J., Sheng S.H., Argon A.S., 2010, *Surface and Coatings Technology* 204, 1898–1906
- 10 - Musil J., 2000, *Surface and Coatings Technology*, 125, 322–330
- 11 - Martínez-Martínez D., López-Cartes C., Justo A., Fernández A., Sánchez-López J.C., 2009, *Solid State Sciences*, 11, 660–670
- 12 - Guimarães F., Oliveira C., Sequeiros E., Torres M., Susano M., Henriques M., Oliveira R., Escobar Galindo R., Carvalho S., Parreira N.M.G., Vaz F., Cavaleiro A., 2008, *Surf. Coat. Tech.*, 202:11, 2403-2407
- 13 - Rai M, Yadav A., Gade A., *Biotechnology Advances*, doi:10.1016/j.biotechadv.2008.09.002
- 14 - Duran N., Macarto P.D., De Sousa G.I.H., Alves O.L., Esposito E., *J. Biomed. Nanotechnol*, 2007, 3 203-207
- 15 - Endrino J.L., Escobar Galindo R., Zhang H.-S., Allen, Gago M.R., Espinosa A., Anders A., *Surf. Coat. Technol.* 2008, 202, 3675-3682
- 16 - Hlídaek P., Hanuš J., Biederman H., Sllavínská D., Pešička J., *Thin Solid Films*, 2008, 516, 4581-4586

17 - Stobie N., Duffy B., McCormack D.E., Colreavy J., Hidalgo M., McHale P., Hinder, S. J., *Biomaterials*, 2008, 29, 963-969

18 - A. Arranz and C. Palacio, *Journal of Physical Chem. B*, 106 (2002) 9590- 9596

19 – Berg S., Nyberg T., 2005, *Thin Solid Films*, 476, 215 – 230

20 – Depla D., Buyle G., Haemers J., Gryse R., 2006, *Surface and Coatings Technology*, 200, 4329-4338

21 – Depla D., Gryse R., 2003, *Vacuum*, 69, 529-536

22 – Petrov I., Barna P.B., Hultmann L., Greene J.E., 2003, *Journal of Vacuum Science Technology A* 21 - 5

23 – Silva E., Rebelo de Figueiredo M., Franz R., Escobar Galindo R., Palacio C., Espinosa A., Calderon S. V., Mitterer C., Carvalho S., 2010 *Surface and Coatings Technology*, 205, 2134–2141

24 – Adamik M., Barna P.B., Tomov I., 1998, *Thin Solid Films*, 317,64-68

25 – Jung I.J., Kang S., 2000, *Journal of Material Science*, 35, 87-90

26 – Dreiling I., Haug A., Holzschuh H., Chassé T., 2009, *Surface and Coatings Technology*, 204, 1008-1012

27 – Constable C.P., Yarwoo J., Munz W.D., 1999, *Surface and Coatings Technology* 116-119, 155-159

28 – Robertson J, 2002, *Materials Science and Engineering*, 37, 129-281

29 – Ferrari A.C., Rodil S.E., Robertson J., 2003, *Diamond and Related Materials*, 12, 905-910

Figure Captions

Fig 1. XPS spectra of Ti 2p core level of TiN, TiC and TiO₂ reference samples

Fig. 2. a) Deposition rate for pure TiCN and Ag-TiCN coatings as function of $J_{TiAg}+J_{Ti}$ for first and second series. b). Evolution of the potential on the targets V_{TiAg} and V_{Ti} as function of $J_{TiAg}+J_{Ti}$ during the deposition of the sample processed with $J_{Ti+Ag} + J_{Ti} = 16 \text{ mA/cm}^2$.

Fig. 3. Ag/Ti atomic ratio versus J_{TiAg}/J_{Ti} ratio for first and second series

Fig. 4. XRD patterns of the pure TiCN and Ag-TiCN coatings deposited by DC reactive magnetron sputtering, with different Ag/Ti atomic ratios.

Fig. 5. TEM micrograph from the cross-section of the Ag-TiCN coatings with Ag/Ti = 0.40 Fig. 5 b) Diffraction pattern from a selected area.

Fig. 6. Cross-sectional SEM micrographs for different atomic ratios Ag/Ti: a) 0 b) 0.20 c) 0.40 d) 1.49 **Inset on Fig 6d) SEM image from the sample surface where are visible Ag clusters.**

Fig.7. XPS spectra of a) Ti 2p b) C 1s c) N 1s d) Ag 3d core levels of the Ag-TiCN coatings deposited by DC reactive magnetron sputtering with different Ag/Ti atomic ratios

Fig. 8. Raman spectra of the Ag-TiCN coatings for different Ag/Ti ratios

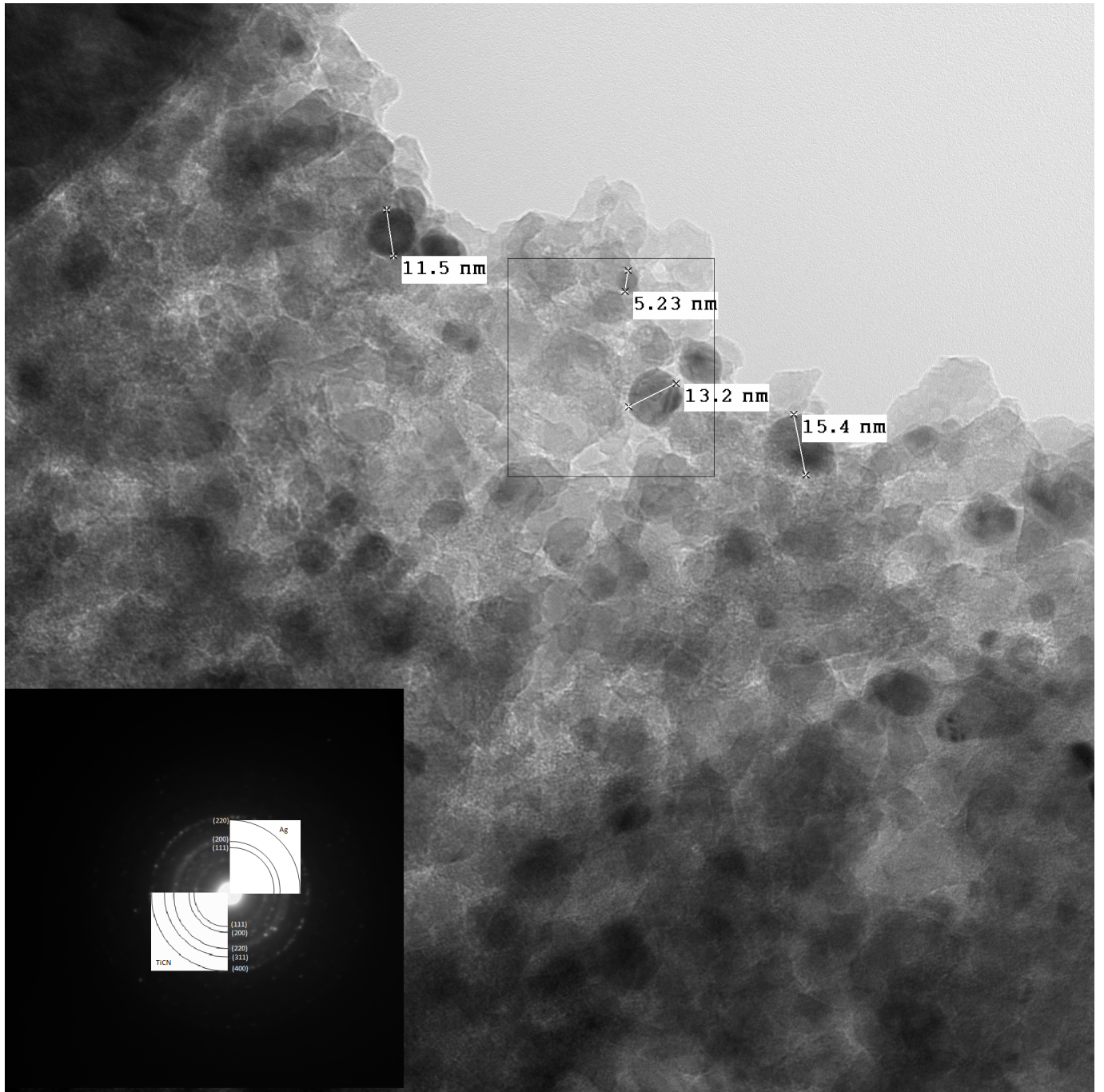


Figure 5 (Fig5corr.tif)

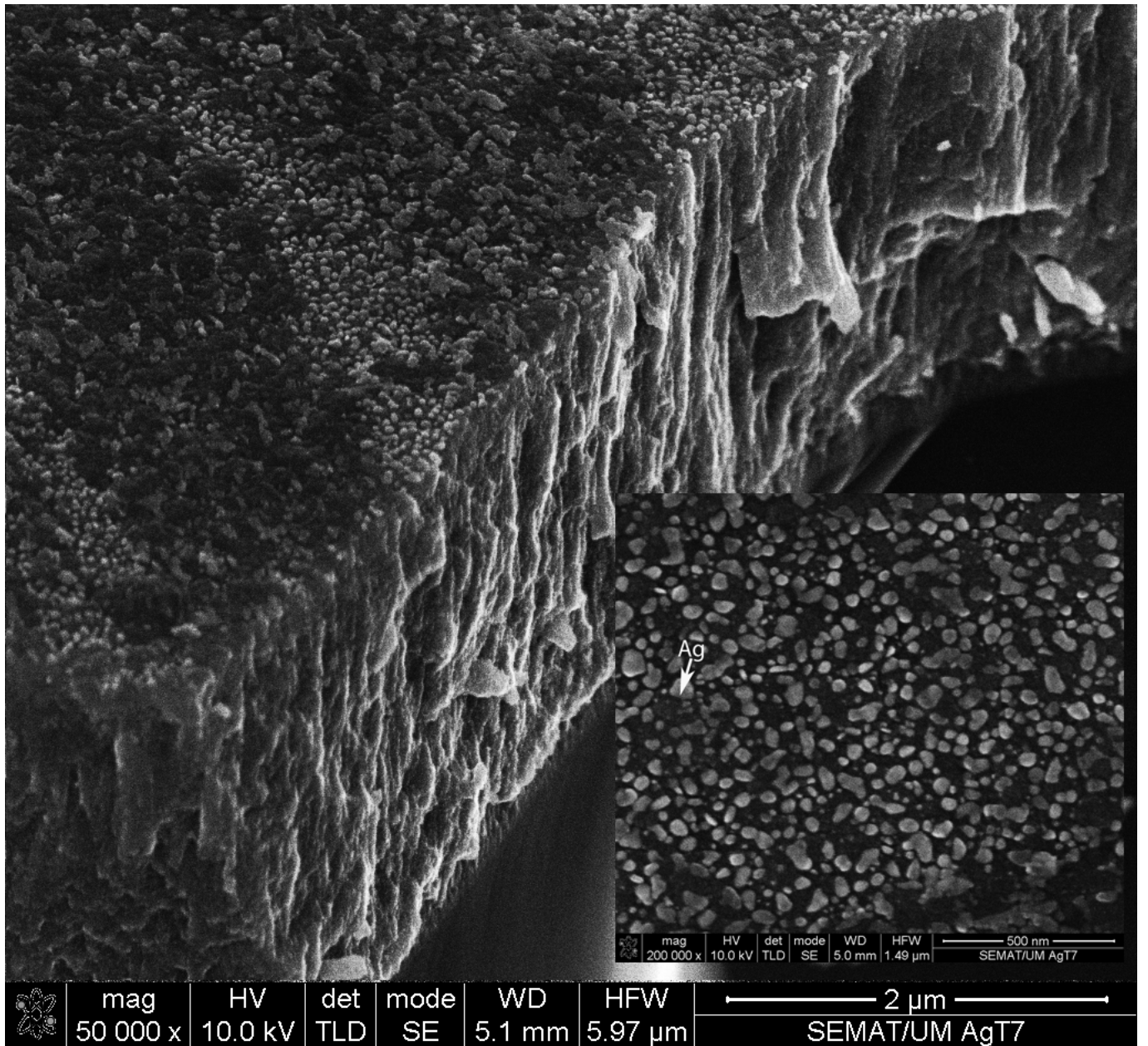


Figure 6d (Fig6dcorr.tif)